Available online at www.sciencedirect.com
ScienceDirect
International Journal of Solids and Structures 45 (2008) 2042–2055
INTERNATIONAL JOURNAL OF SOLIDS AND STRUCTURES
www.elsevier.com/locate/ijsolstr

Analytical and numerical analysis of sheet metal instability using a stress based criterion

Hagbart S. Alsos [a,*], Odd S. Hopperstad [b], Rikard Törnqvist [c], Jørgen Amdahl [a]

[a] Department of Marine Technology, Norwegian University of Science and Technology, Otto Nielsens V. 10, 7491 Trondheim, Norway
[b] Structural Impact Laboratory (SIMLab), Centre for Research-based Innovation, Department of Structural Engineering, Norwegian University of Science and Technology, Richard Birkelandsv. 1a, 7491 Trondheim, Norway
[c] DNV Energy, Veritasveien 1, 1322 Høvik, Norway

Received 26 July 2007; received in revised form 12 October 2007
Available online 5 December 2007

Abstract

Strain based Keeler–Goodwin diagrams are widely used in forming processes to predict onset of local necking. Plastic instability is determined once the forming limit strain is exceeded. Use of these diagrams requires proportional strain paths, which is not necessarily the case in sheet metal forming operations. In many forming processes, the strain path changes during deformation. This may change the forming limit curve significantly. In the paper, a stress based forming limit criterion is adopted to deal with strain path non-linearities. Comparisons with earlier published work on forming limits are made through analytical considerations. Furthermore, the criterion is implemented into the finite element code LS-DYNA and verified numerically against results from large scale bulge tests.

Keywords: Material instability; Local necking; Fracture; Pre-straining; Finite element analysis; Shell elements

1. Introduction

Reasonable prediction of fracture is important when exploring the limits of metal sheets. Not only is this true for metal forming processes, but also in crashworthiness analyses where failure may significantly reduce the resistance of a structure. In industrial forming processes, the Keeler–Goodwin approach, see Keeler and Backhofen (1964) and Goodwin (1968), has been the dominating method of estimating failure for many years. In this method, the principal strains (ϵ_1, ϵ_2) at incipient plastic instability are plotted in a forming limit diagram (FLD). An example of such a diagram is illustrated in Fig. 1.

Proportional strain paths are assumed when establishing the FLD. This means that the ratio β between the minor principal strain rate $\dot{\epsilon}_2$ and major principal strain rate $\dot{\epsilon}_1$ remains constant during deformation. This is not necessarily the case in processes where large deformation takes place, e.g., industrial metal forming

* Corresponding author. Tel.: +47 735 50446.
E-mail address: hagbarts@ntnu.no (H.S. Alsos).

0020-7683/$ - see front matter
doi:10.1016/j.ijsolstr.2007.11.015

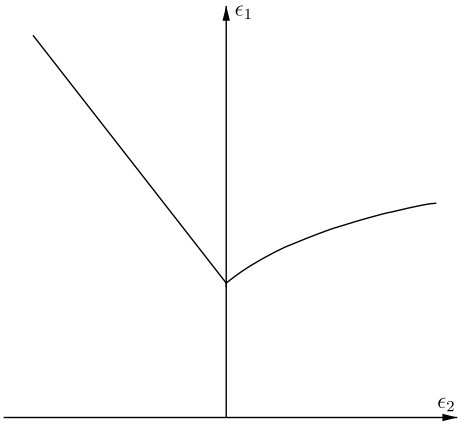

Fig. 1. Typical forming limit diagram.

applications and sheet metal deformation in collision processes. Due to various effects, such as material hardening, changed specimen geometry and contact, the loading path may alter. It has been reported by several authors that non-proportional strain paths may change the forming limits of materials, e.g., Ghosh and Laukonis (1976) and Graf and Hosford (1993). An arising awareness of this effect became apparent during the 1970s, through FLDs derived from experiments on pre-strained specimens, e.g., Ghosh and Laukonis (1976). Later documentation on this was published during the 1980s and 1990s, see for example Rocha et al. (1985), Graf and Hosford (1993). Although its generality may be questioned, the Keeler–Goodwin method has not changed much from its initial form. Reasons for this may be that FLDs are intuitive and easy to use. More complex methods require more resources, both from computers and the ones applying them.

A simple alternative to strain based FLDs is stress based FLDs. Such diagrams were first presented by Arrieux et al. (1982), and later by Stoughton (2000, 2001), Stoughton and Zhu (2004) and Wu et al. (2005). The idea is that stress based criteria remains more or less unaffected by altered strain paths. Furthermore, the nature of this type of formulation is simple and easily implemented into a finite element (FE) code.

This paper adopts the stress based forming limit approach and evaluates a combined Hill (1952) and Bressan and Williams (1983) instability criterion, here referred to as the BWH criterion. The BWH criterion is meant to offer a simplified way to estimate the onset of local necking. The verification of the BWH criterion is carried out in two separate series of analyses. The first one is a set of analytical considerations, which is compared with FLDs found in literature. The second set of analyses is performed numerically using the finite element code LS-DYNA, see Hallquist (2007a,b). The finite element simulations are further compared with benchmark tests (large scale bulge tests) provided by Törnqvist (2003).

2. The BWH instability criterion

The forming limit diagram, as it is most often presented, is an intuitive way of displaying the limits of materials. However, as it has been highlighted, it is only strictly valid for proportional straining, i.e., the strain rate ratio $\beta = \dot{\epsilon}_2/\dot{\epsilon}_1$ remains constant. Ghosh and Laukonis (1976) and Graf and Hosford (1993) have shown that for non-linear strain paths, the FLD may change. One simplified way of circumventing this problem is to adopt stress based forming limit curves (FLC). This methodology has been strongly argumented for by Stoughton, see for example Stoughton (2000, 2001) and Stoughton and Zhu (2004). Stresses can be directly coupled to the plastic strain rates through the relations between the strain rates and the conditions for yielding and plastic flow. If the yield function and the potential for plastic flow are assumed identical, the relations between strain rates and stresses can be found from the associated flow rule

$$\dot{\epsilon}_{ij} = \dot{\lambda}\frac{\partial f}{\partial \sigma_{ij}} \tag{1}$$

where $\dot{\epsilon}_{ij}$ and σ_{ij} denotes plastic strain rate and stress tensor on index form, $\dot{\lambda}$ is the plastic multiplier, and f describes the yield function. If J_2 flow theory and plane stress conditions are assumed, the relation between the strain rate ratio β and the principal stresses σ_1 and σ_2 can be expressed as

$$\alpha = \frac{\sigma_2}{\sigma_1} = \frac{1+2\beta}{\beta+2} \tag{2}$$

Note that this relation is valid for plastic strains only. Elastic strains are neglected, which is reasonable since plastic strains are much larger. In Fig. 2, an example of a strain based FLD (a) and a stress FLD (b) is shown. The difference between these is that the stress based FLC remains fixed in the stress space for non-linear strain paths, while the strain based FLC may change for various combinations of non-proportional straining.

2.1. Hill's local necking criterion

Hill (1952) proposed a criterion for local necking in the negative β regime. He assumed that a local neck will form with an angle ϕ to the direction of the major principal stress. Within this neck, the strain increments along the narrow necking band will be zero. The orientation of the neck may be expressed as $\phi = \tan^{-1}\left(1/\sqrt{-\beta}\right)$, which yields rational results only for negative values of β. At the instant a neck is formed, the effects from strain hardening and the diminution in thickness balance each other exactly. This means that the fractions within the material reach a maximum value at the point of local necking. This gives traction increments equal to zero, $\mathrm{d}T_1 = 0$, at the point of necking, which leads to the following local necking criterion

$$\frac{\mathrm{d}\sigma_1}{\mathrm{d}\epsilon_1} = \sigma_1(1+\beta) \tag{3}$$

Assuming that the material stress–strain curve can be represented by the powerlaw expression, $\sigma_{\mathrm{eq}} = K\epsilon_{\mathrm{eq}}^n$, where (K, n) are material parameters and $(\sigma_{\mathrm{eq}}, \epsilon_{\mathrm{eq}})$ are the equivalent stress and strain, and that proportionality between stress rates and stresses can be assumed, i.e.,

$$\alpha = \frac{\dot{\sigma}_2}{\dot{\sigma}_1} = \frac{\sigma_2}{\sigma_1},$$

the equivalent strain at local necking can be expressed as

$$\epsilon_{\mathrm{eq}} = \frac{2n}{\sqrt{3}} \frac{\sqrt{\beta^2+\beta+1}}{1+\beta} \tag{4}$$

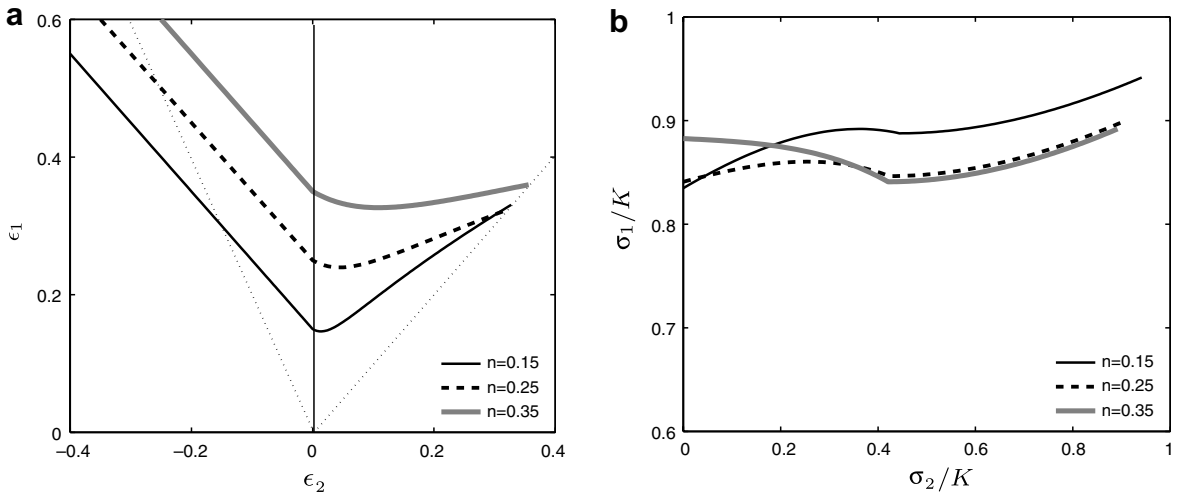

Fig. 2. Forming limit diagrams in (a) strain space, (b) stress space. Both figures illustrate the same materials. Note that the figure (b) is normalized by the powerlaw parameter K in $\sigma_{\mathrm{eq}} = K\epsilon_{\mathrm{eq}}^n$, where $(\sigma_{\mathrm{eq}}, \epsilon_{\mathrm{eq}})$ are the equivalent stress and strain, and n is the powerlaw exponent.

If proportional straining is assumed, the familiar strain based Hill's expression appears

$$\epsilon_1^* = \frac{\hat{\epsilon}_1}{1+\beta} \tag{5}$$

Here $\hat{\epsilon}_1$ is equal to the powerlaw exponent n, although measured values may sometimes yield better correlation with experiments. As equation Eq. (5) is based on proportionality it has limited use. Alternatively, a path independent stress based FLC may be found directly from Eq. (4) and the powerlaw expression. This gives the equivalent stress at local necking (note that also here $\hat{\epsilon}_1$ refers to the powerlaw exponent n)

$$\sigma_{\text{eq}} = K\left(\frac{2\hat{\epsilon}_1}{\sqrt{3}}\frac{\sqrt{\beta^2+\beta+1}}{1+\beta}\right)^n \tag{6}$$

This results in the following major principal stress

$$\sigma_1 = \frac{2K}{\sqrt{3}}\frac{1+\frac{1}{2}\beta}{\sqrt{\beta^2+\beta+1}}\left(\frac{2}{\sqrt{3}}\frac{\hat{\epsilon}_1}{1+\beta}\sqrt{\beta^2+\beta+1}\right)^n \tag{7}$$

A similar derivation has been shown by Stoughton and Zhu (2004).

2.2. The Bressan–Williams shear instability criterion

Hill's local necking criterion yields only rational results for negative β values. In the positive regime, other methods of estimating the onset of local necking are needed. A popular solution to this goes through the methodology established by Marciniak and Kuczynski (1967) (M–K). This procedure introduces pre-existing defects within the material, which trigger local necking. The defects are often introduced as a groove within a material element. During deformation, the strain field is solved incrementally. Local necking is initiated once the material within the groove starts to strain at a significantly higher rate than the surrounding material and the strain rate ratio β within the emerging neck approaches zero (plane strain). The M–K method describes in a physical way the initial stage of local necking and as for stress based approaches, it does handle non-proportional straining. The drawback, however, is that it becomes computationally demanding if used in finite element analyses. Either one has to apply a high number of small elements in order to include small imperfections, or the M–K procedure needs to be introduced into each finite element. Hence, a much simpler stress based instability criterion known as the Bressan–Williams criterion (BW) is adopted, Bressan and Williams (1983). Contrary to the M–K method, the BW criterion may be solved analytically and can be used for failure estimation with reasonable precision at a low cost.

In plasticity, the main mechanism of deformation comes from slip arising from shear on certain preferred combinations of crystallographic planes. Furthermore, it has been observed by experiments that failure planes in sheet metal lie close to the direction of maximum shear stress, see Bressan and Williams (1983). It is therefore reasonable to assume that the instability may take place before any visual signs of local necking. Thus, a shear stress based instability criterion may well be useful in estimating the point of local necking. As presented by Bressan and Williams (1983), the BW criterion has a simple expression and has been applied with good results. The basis for the BW expression follows three basic assumptions. First of all, the shear instability is initiated in the direction through the thickness at which the material element experiences no change of length. This indicates a critical through thickness shear direction. Secondly, the instability is triggered by a local shear stress which exceeds a critical value. This means that the initiation of local necking is described as a material property. Finally, elastic strains are neglected. This is reasonable since the elastic strains are small compared to the plastic strains at local necking.

From Fig. 3, and from the assumptions above, a mathematical formulation for the BW criterion can be found. As illustrated in Fig. 3a, the inclined plane through the element thickness at which shear instability occurs (indicated by the plane normal x_n) forms an angle $\pi/2-\theta$ to the shell plane. The material experiences zero elongation in this direction, indicating that $\dot{\epsilon}_t = 0$. This gives the following relation between the angle of the inclined plane and the principal strain rates

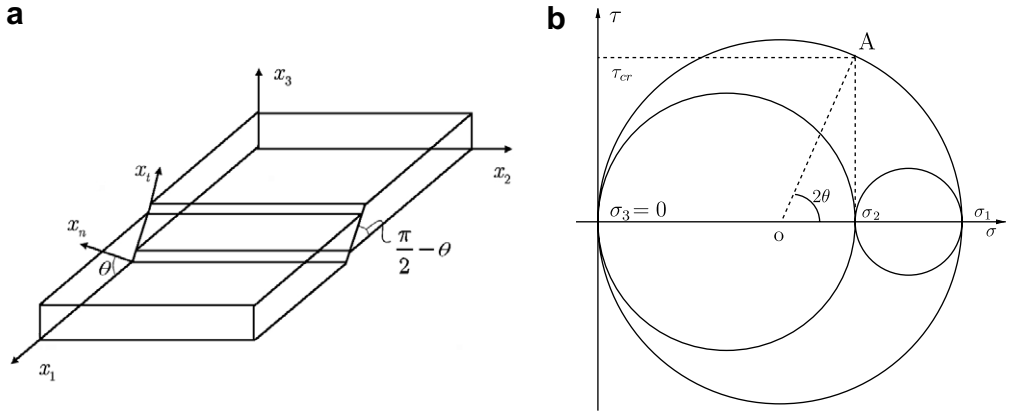

Fig. 3. (a) Local shear instability in a material element. Note that no elongation takes place in the x_t direction. (b) Shows the stress components in a Mohr's circle.

$$\dot{\epsilon}_t = \frac{\dot{\epsilon}_1 + \dot{\epsilon}_3}{2} + \frac{\dot{\epsilon}_1 - \dot{\epsilon}_3}{2}\cos 2\left(\theta + \frac{\pi}{2}\right) = 0 \tag{8}$$

where $\cos 2(\theta + \pi/2) = -\cos 2\theta$, which further gives

$$\cos 2\theta = \frac{\dot{\epsilon}_1 + \dot{\epsilon}_3}{\dot{\epsilon}_1 - \dot{\epsilon}_3} \tag{9}$$

Assuming plastic incompressibility, $\dot{\epsilon}_3 = -\dot{\epsilon}_1(1+\beta)$, the angle θ can be found as a function of the ratio β

$$\cos 2\theta = -\frac{\beta}{2+\beta} \tag{10}$$

The corresponding stress state can be obtained from the rules of stress transformation, or simply by drawing up Mohr's circle, Fig. 3b. This gives the following relation between the inclined plane and the stresses involved

$$\tau_{cr} = \frac{\sigma_1}{2}\sin 2\theta \tag{11}$$

where τ_{cr} is the critical shear stress. Finally, Eq. (10) and (11) may be combined into the expression which gives the BW criterion

$$\sigma_1 = \frac{2\tau_{cr}}{\sqrt{1-\left(\frac{\beta}{2+\beta}\right)^2}} \tag{12}$$

A similar derivation is given by Brunet and Clerc (2007). Bressan and Williams initially suggested calibration either from uniaxial tensile tests or biaxial tests. Another alternative may be calibration at plane strain, $\beta = 0$, through notched specimens or simply from Hill's analysis. If the BW criterion is calibrated from Hill's expression at plane strain, Eq. (7), the critical BW shear stress takes the following form

$$\tau_{cr} = \frac{1}{\sqrt{3}}K\left(\frac{2}{\sqrt{3}}\hat{\epsilon}_1\right)^n \tag{13}$$

Also here, $\hat{\epsilon}_1$ is equal to the powerlaw exponent n.

2.3. The Bressan–Williams–Hill criterion

The BW criterion was initially intended for the positive quadrant of the FLD, but the mathematical expression is also valid for negative values. However, as the strain rate ratio becomes negative, the validity of the BW criterion becomes questionable. Hence, in order to cover the full range of β, the Hill and BW criteria have been

combined into one criterion, from now on referred to as the BWH criterion. Formulated in terms of the strain rate ratio, β, the criterion reads

$$\sigma_1 = \begin{cases} \frac{2K}{\sqrt{3}} \frac{1+\frac{1}{2}\beta}{\sqrt{\beta^2+\beta+1}} \left(\frac{2}{\sqrt{3}} \frac{\hat{\epsilon}_1}{1+\beta} \sqrt{\beta^2+\beta+1} \right)^n, & \text{if } \beta \leqslant 0 \\ \frac{2}{\sqrt{3}} K \frac{\left(\frac{2}{\sqrt{3}} \hat{\epsilon}_1 \right)^n}{\sqrt{1-\left(\frac{\beta}{2+\beta} \right)^2}}, & \text{otherwise} \end{cases} \tag{14}$$

The BWH criterion is illustrated in both strain and stress space in Fig. 2 for various hardening exponents, n.

3. Analytical validation of the BWH criterion

A strong argument for the BWH criterion, is that it can be applied analytically to develop FLDs. This goes for both proportional straining as well as for non-proportional straining. As a part of the validation process, the BWH criterion is used to determine FLDs in a set of benchmark cases. The BWH forming limit diagrams have then been compared with FLDs found in literature, e.g., Graf and Hosford (1993), Rocha et al. (1985), Brunet and Morestin (2001) and Stoughton (2000). Common to all of these is the focus on the effect of non-linear strain paths. This is done through forming limit analyses of pre-strained specimens.

3.1. Comparison with pre-strained Al 2008 T4

Graf and Hosford (1993) investigated the effect of non-linear strain paths in Al 2008 T4. The specimens were first pre-strained in uniaxial, plane strain and equi-biaxial tension. Thereafter FLCs were generated. These are illustrated in Fig. 4a and show how the forming limit changes with the degree of pre-straining. In Graf and Hosford's experiments, specimens of equi-biaxial pre-strain levels of 0%, 4%, 7%, 12%, and 17% were used. The results clearly show that the strain path does have an effect on the forming limit curve. A similar series of tests were conducted by Graf and Hosford (1994) at a later stage for Al 6111 T4. The same trend as for Al 2008 T4 was observed.

In Fig. 4b, the response of Al 2008 T4 is investigated by using the BWH criterion. The material is reported to follow the powerlaw over the strain range 5–20%, using the parameters $K = 593$ MPa and $n = 0.285$. For accuracy reasons, the $\hat{\epsilon}_1$ parameter is calibrated to a different value than that given by the powerlaw exponent, n. Fig. 4a shows that the major principal strain at local necking in plane strain is equal to 0.19, hence $\hat{\epsilon}_1 = 0.19$.

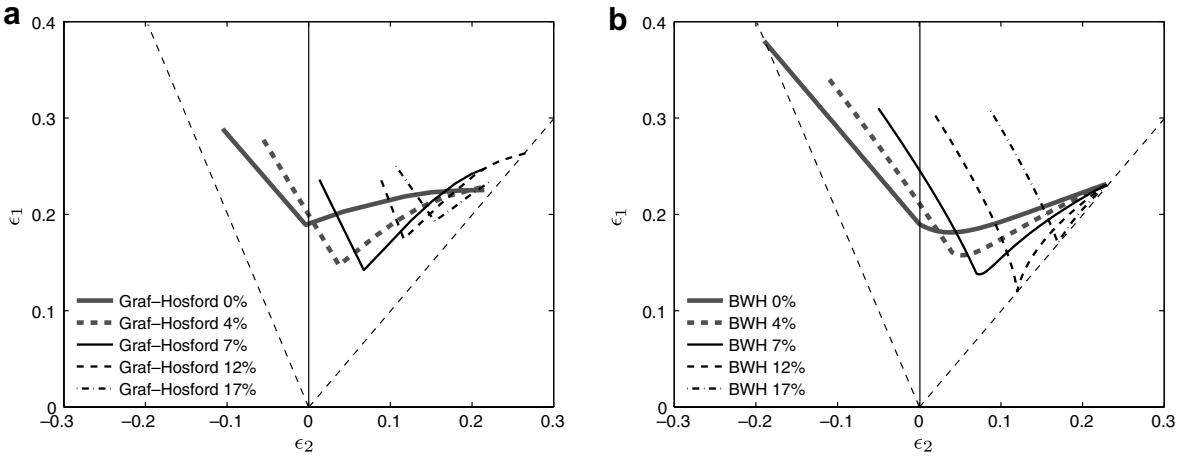

Fig. 4. Strain based FLD. In (a), data from Graf and Hosford (1993) for biaxially pre-strained material, (b) FLDs obtained with the BWH criterion.

When comparing the diagrams in Fig. 4a and b, the curves correlate well. Clearly, the BWH criterion is able to account for non-linear strain paths introduced by the pre-strains.

Stoughton (2000) studied the effect of non-proportional straining on stress based FLCs using Graf and Hosford's data. By using Hill's 1948 model for plastic potential, he mapped Graf and Hosford's FLDs for Al 2008 T4 into the stress space. The results are shown in Fig. 5 together with the BWH curve for the same material. As the figure shows, the stress data fall close together. This may indicate that the forming limit in stress space, remains more or less unaffected by the strain path, hence the expression "strain path independency". Wu et al. (2005) have also made similar observations. This is an argument which speaks for stress based forming limit criteria.

3.2. Comparison with pre-strained ARMCO iron

Rocha et al. (1985) investigated how pre-straining and the degree of anisotropy affected the forming limit of ARMCO iron. In their analyses, the material was assumed to have orthotropic symmetry which was accounted for by Hill's plastic potential, Hill (1950). The local necking analyses were carried out by following

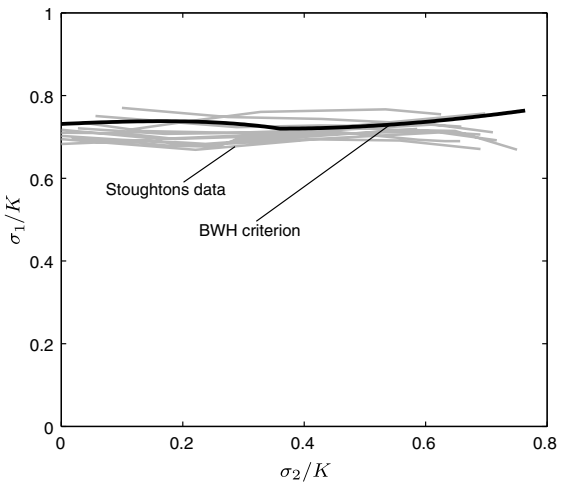

Fig. 5. Stress based FLD. In gray, data from Stoughton (2000), in black, results obtained with the BWH criterion.

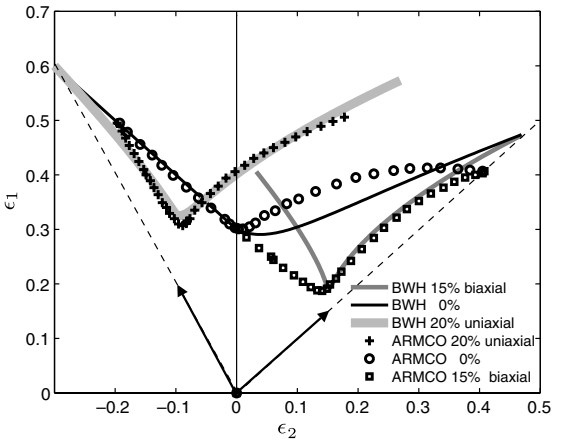

Fig. 6. Forming limit for pre-strained material, experiments by Gronostajski et al. (1982) versus results obtained with the BWH criterion.

the framework provided by Marciniak and Kuczynski (1967). The results of their analyses were then compared with experimental results provided by Gronostajski et al. (1982).

Rocha et al. (1985) reported a stress–strain curve which followed the powerlaw using a powerlaw exponent $n = 0.2$. The ARMCO iron is, however, more ductile than the powerlaw exponent indicates. If not pre-strained, the FLD in Fig. 6, intersects with the ϵ_1 axis at $\epsilon_1 = 0.3$. $\hat{\epsilon}_1$ is therefore set equal to 0.3.

In Fig. 6, a set of BWH produced FLCs is compared with forming limit data for ARMCO iron, Gronostajski et al. (1982). Forming limit curves for the virgin material and for two levels of pre-strain are shown. These are 20% uniaxial pre-straining and 15% equi-biaxial pre-straining. Also here the forming limit is affected by the non-proportional strain history.

As Fig. 6 shows, the correlation between experimental and analytical curves is surprisingly good. The most significant deviation is found on the left hand side of the FLC for the equi-biaxially pre-strained material. Deviation is also seen at the right hand side for the virgin material. Similar deviations can also be seen in analyses presented by Rocha et al. (1985).

3.3. Comparison with pre-strained mild steel

In this sub section, forming limit diagrams presented by Brunet and Morestin (2001) are compared with FLDs acquired through considerations of the BWH criterion. The benchmark FLDs have been developed through experimental testing and numerical analyses of pre-strained mild steel (Fep04).

In the numerical analyses, Brunet and Morestin reported a material following the powerlaw with parameters, $K = 521$ MPa and $n = 0.24$. In addition to a virgin material configuration, two pre-strained configurations were identified. These are pre-straining in uniaxial tension and equi-biaxial tension, with strain values at 10% and 15%, respectively. As shown in Fig. 7a, the FLD for the virgin material yields a major principal limit strain of 0.3 at plane strain. Thus, $\hat{\epsilon}_1 = 0.3$. The comparison between Brunet and Morestin's experimental and numerical predictions, and the predictions made using the BWH criterion is illustrated in Fig. 7. The correlation between the results obtained with the BWH criterion and the other FLCs is satisfactory.

It is important to keep in mind that all the results provided by the BWH criterion are based on simple J_2 flow theory. Furthermore, the only input to the BWH criterion comes from the hardening of the material and the local necking strain at plane strain. Hence, the BWH model is a simplified instability criterion, which in this paper is intended for fast prediction of the onset of local necking.

4. Numerical comparison with experiments – The "giant bulge" test

The simple formulation of the BWH criterion makes it ideal for prediction of plastic instability in finite element analyses, especially if the elements used in the simulation are larger than the scale of the instability itself. In this way, the BWH criterion may be able to efficiently estimate the onset of instability at a reasonable computational cost.

The BWH criterion has been implemented into the finite element code LS-DYNA and used in a set of large scale bulge simulations. The simulation results have so been compared to the identical set of experimental results, here referred to as the "giant bulge tests".

4.1. The "giant bulge" test

The large scale bulge tests were carried out by Törnqvist (2003), as a part of a study on the RTCL damage criterion (Rice and Tracey (1969) and Cockcroft and Latham (1968) damage criterion). The bulge tests were performed on large circular specimens bolted to a pressure device. The diameter of the overall setup was more than one meter, and the plates varied from 5 mm thick steel plates to more than 10 mm thick aluminum plates. As the name implies, the plates were forced to bulge as they were loaded. This was made possible by a large oil pressure on one side, and a large die on the other side. As a contrast to punching tests, the deformation was enforced without the disturbance from friction.

Törnqvist carried out experiments on various specimen configurations. As mentioned, both steel and aluminum plates were considered. This was done both for undamaged plates as well as for surface cracked spec-

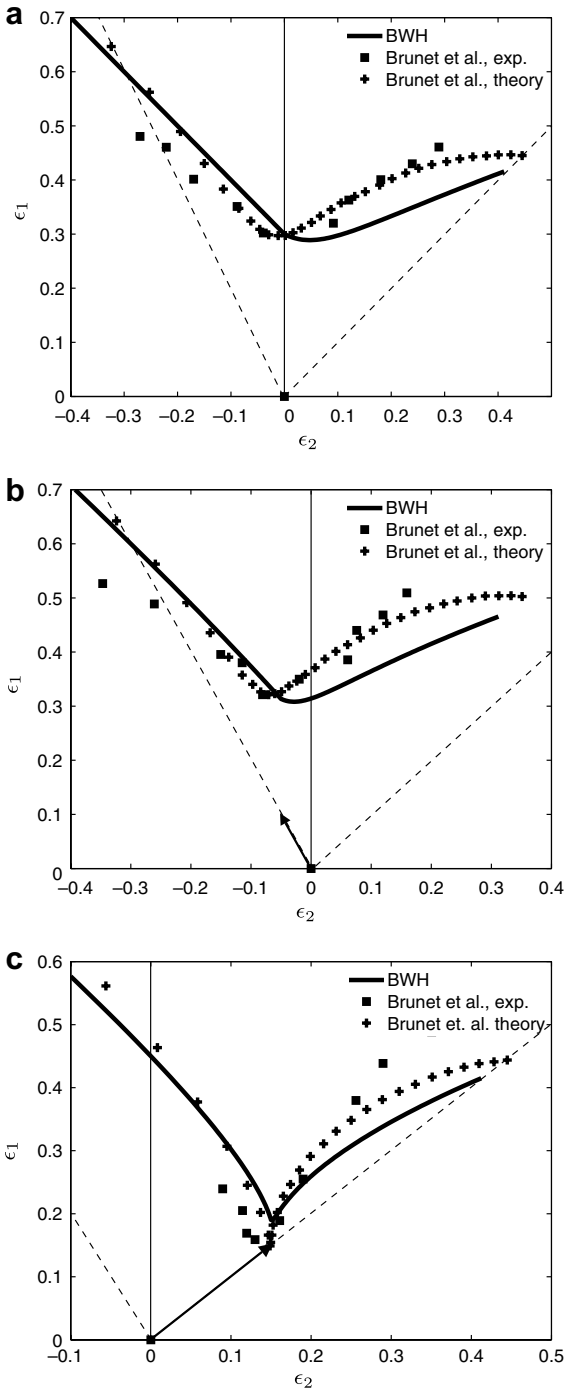

Fig. 7. FLDs obtained with the BWH criterion compared with data provided by Brunet and Morestin (2001) in (a) virgin material, (b) 10% uniaxial pre-straining, and (c) 15 % biaxial pre-straining.

imens. For further information, see Törnqvist (2003). In this paper, only undamaged steel plates with a plate thickness of 5 mm are considered.

The experiments were performed using both elliptic and circular dies, Fig. 8. In this way, two different stress states were produced. The circular specimen had a plate and die diameter equal to 960 mm. The die itself was

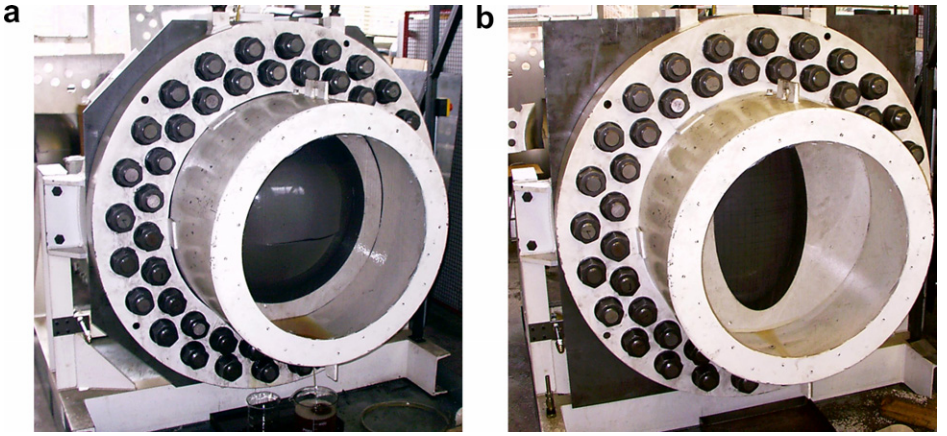

Fig. 8. Photos of the experiments showing, (a) circular plate and die, (b) elliptic plate and die.

shaped like a torus with a rim radius of 125 mm. The elliptic specimen also resembled the torus geometry, although with different diameters in the horizontal plane. The major and minor diameters of the ellipse were 960 and 580 mm, and the rim radius was equal to 150 mm. The test setup is shown in Fig. 8 and the FE models are illustrated in Fig. 9.

4.2. Material and FE model

The plate specimens were manufactured from mild steel, EN 10025 S275, which resembles a typical structural steel. The stress–strain curve for the material is shown in Fig. 10. The shape of the curve, and especially the plateau at first yield, is very characteristic to steel. Hence, to obtain an accurate representation with the powerlaw, some modifications are made. In the following simulations, the yield plateau is included by introducing the powerlaw as a step function which is initiated at the end of the yield plateau. This gives the following modified powerlaw expression

$$\sigma_{\text{eq}} = \begin{cases} \sigma_Y, & \text{if} \quad \epsilon_{\text{eq}} \leqslant \epsilon_{\text{plat}} \\ K(\epsilon_{\text{eq}} - \epsilon_0)^n, & \text{otherwise} \end{cases} \tag{15}$$

where ϵ_{plat} is the equivalent plastic strain at the plateau exit and σ_Y the initial yield stress. ϵ_0 describes a modified plateau strain which allows the plateau and powerlaw expression to intersect at $(\epsilon_{\text{plat}}, \sigma_Y)$. This is formulated as

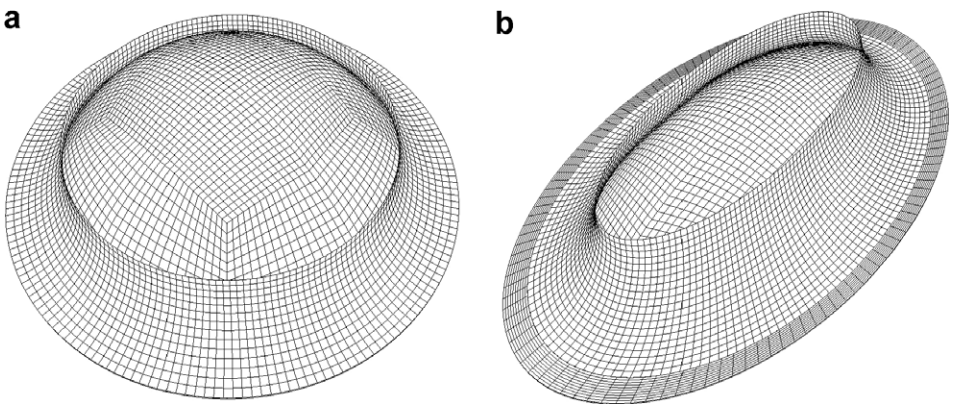

Fig. 9. Finite element bulge models, (a) circular plate and die, (b) elliptic plate and die.

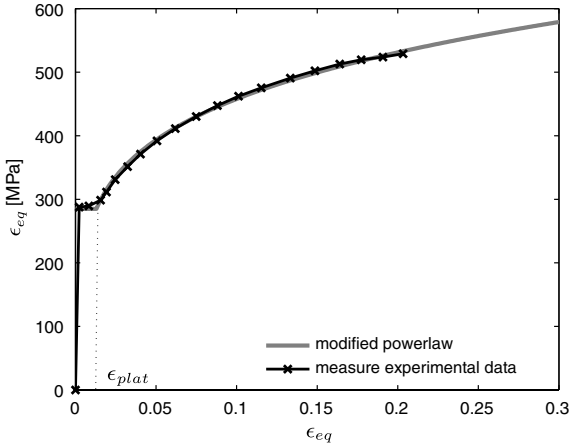

Fig. 10. True stress–strain curves for the mild steel (EN 10025 S275). Both experimental datapoints and the powerlaw fit are shown.

$$\epsilon_0 = \epsilon_{\text{plat}} - \left(\frac{\sigma_Y}{K}\right)^{\frac{1}{n}} \tag{16}$$

Although a modified powerlaw expression is used for the stress–strain representation, the BWH criterion remains as in Eq. (14).

In the analyses, little is known about the local necking properties of the material, hence $\hat{\epsilon}_1$ is set equal to the hardening exponent n. The stress–strain curve is represented by the following values, yield stress $\sigma_Y = 290$ MPa, plateau strain, $\epsilon_{\text{plat}} = 0.011$, and the powerlaw parameters (K, n) equal to 730 MPa and 0.19, respectively.

The finite element models are meshed with several grades of fineness in order to investigate the degree of mesh sensitivity, ranging from small element dimensions of 2.5 mm to length of 25 mm. The element used herein is the one point quadrature Belytschko–Lin–Tsay shell element, Belytschko et al. (1984). It is well worth noticing that this element uses discrete Mindlin shell theory to describe displacements and rotations, Belytschko et al. (1984, 2004). Shear strains and stresses through the shell thickness are however small and therefore neglected in analyses with the BWH criterion. In order to account for any roughness in the plate surface, and to promote inception of local necking, the element thickness is randomized according to a Gauss distribution with standard deviation equal to 0.001 times the plate thickness.

Element failure is based on the middle through thickness integration points to avoid effects from bending. This implies that pure plate bending will not cause local necking. It is, however, possible that introducing failure in this way may be too conservative. It has been shown by Tarrett and Stoughton (2003) that specimens subjected to a combination of bending and tension must exceed the forming limit for all layers through the thickness. Hence, simulations which agreed to the latter observation were also performed. However, the difference in results is small, primarily because the problem is dominated by membrane stretching.

In addition to the numerical reproduction of the bulge tests, a series of uniaxial tensile simulations has also been performed. This is done both for verification of the powerlaw parameters and to explore the behavior of the BWH criterion in the left FLD quadrant. The tensile tests were performed on identical plate qualities as the bulge test, with gauge length 90 mm and width 30 mm. In the numerical analyses, the tensile specimens are meshed with different element sizes in order explore the degree of mesh size effect. The characteristic element length is significantly smaller than in the bulge test, because of much smaller specimen dimensions. Three element sizes are used, i.e., characteristic lengths of 1, 2.5, and 5 mm respectively.

4.3. Experimental and numerical results

The bulge tests were deformed as a reaction of a controllable oil pressure behind the steel plate. A natural way to address the load deformation parameters is therefore through oil filling (increase in volume due to plate bulging) and oil pressure behind the bulge.

The plate controlled by the circular die reached a maximum pressure of 8.91 MPa at an added volume of 73 L. The pressure then dropped slightly before the point of fracture, i.e., filling volume of 78 L. The pressurized area in the elliptic die was smaller than for the circular die. This generated higher pressures at lower filling values before fracture occurred. The rupture pressure for the elliptic configuration was 13.2 MPa at an added volume of 25 L.

The results of the simulations are compared with the experimental data in Fig. 11. The simulations correlate well with the experiments, and show no obvious tendency of element size sensitivity. Failure is initiated right before the actual fracture takes place, but well within the acceptable failure range. This is especially true when recognizing that the BWH criterion predicts local instability rather than the state of final fracture, and that the only input data are the parameters of the powerlaw.

Fig. 12 shows the deformed specimens which have been extracted from the simulations. The shaded plot illustrates the value of strain rate ratio β. The darker zones, indicate a large degree of biaxial straining, while the lighter areas indicate β values closer to plane strain. The highest level of β is seen in the circular test. Throughout the process β remains stable and uniform in the proximity of the specimen center. Here, β is close to unity, i.e., equi-biaxial loading. Right before failure, the strain rate ratio, β, is seen to drop towards zero, indicating plane strain in the failing elements. The elliptic test shows a slightly different deformation pattern. The average β value throughout the process is close to 0.4. However, at the "edges" along the major axis of the ellipse, the β value is significantly higher. Failure appears in the middle of the specimen. Here, β goes from an early value greater than 0.5 and drops below 0.3 right before failure.

The results of the tensile test simulations are shown in Fig. 13. The load-displacement data are transformed into measures of engineering strains and stresses, due to convenience reasons. Naturally, the correlation prior to diffuse and local necking is good. This is to be expected, since deformations are relatively low and uniformly distributed over the whole specimen. After the onset of local necking, the responses of the differently meshed models are deviating. This is also expected, due to the high strain concentrations and the lack of through thickness resistance in the elements within the local neck. Hence, the failure strains found from shell analysis in the post necking phase display unphysical values, which will vary with the mesh size. It is however interesting to observe that the BWH criterion predicts failure right at the separation point for all meshes. At this point, the strain rate ratio β in the failing elements are seen to increase from a value of -0.5 (uniaxial stress) towards zero (plane strain). This indicates that the criterion is able to predict the point of instability for all meshes. Furthermore, this means that the criterion predicts failure without being too sensitive to the mesh size. This is both convenient and consistent with the plane stress behavior of shell models.

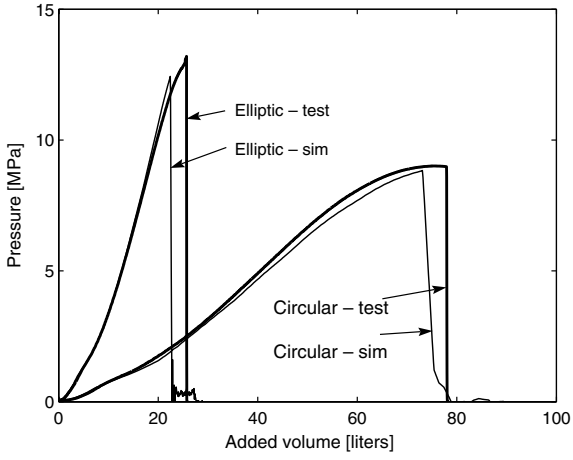

Fig. 11. Pressure vs added volume, experimental and simulation results.

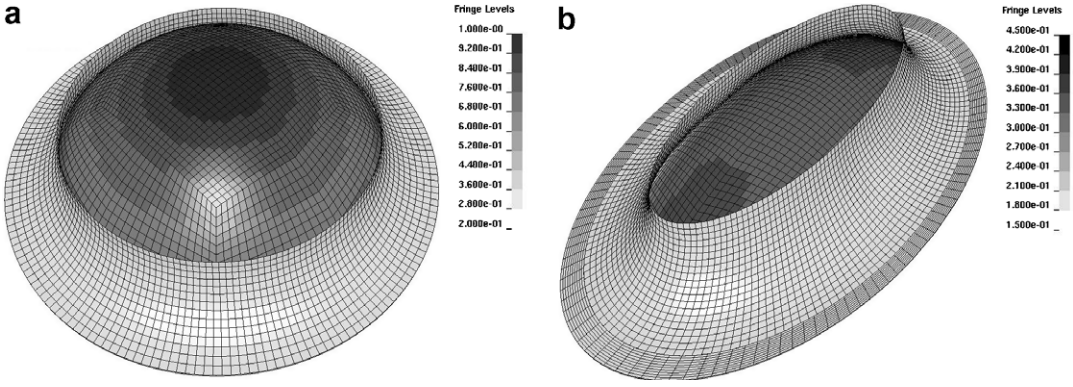

Fig. 12. Deformed mesh and β values right before failure, (a) circular plate and die, (b) elliptic plate and die.

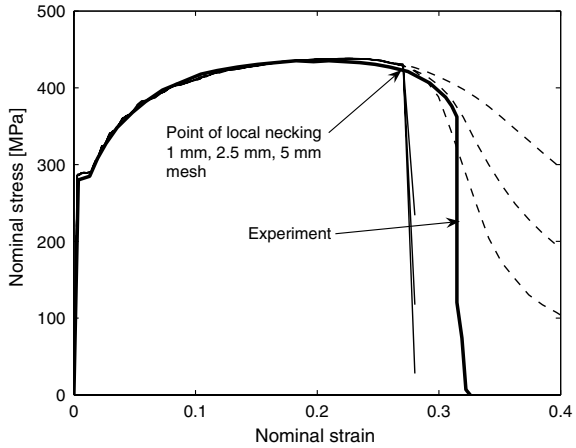

Fig. 13. Tensile test compared with shell element simulations using the BWH criterion for three different mesh sizes. Stapled lines indicate simulations without fracture, while the thin lines indicate simulations with fracture.

5. Discussion and conclusions

The BWH criterion is used in analysis of plastic instability and performs well compared to the benchmark FLDs. The criterion explicitly gives the limit value based on the powerlaw hardening exponent, n, and some measured critical strain, $\hat{\epsilon}_1$. In this paper, this value is the local necking strain at plane strain, $\beta = 0$. However, reasonable failure estimations can be made if calibration is made according to Hill's analysis of local necking, $\hat{\epsilon}_1 = n$. All analyses performed herein are based upon the assumption of plastic isotropy and J_2 flow theory. Thus, considering the coarse data available, the results are satisfactory.

The BWH criterion may easily be implemented into a finite element code. The simple nature of the criterion makes it very CPU efficient and attractive in analysis of structures where material and failure data are limited, e.g., simple estimations on forming operations, crashworthiness analyses and accidental analysis involving large scale structures. Many of these analyses applies relatively coarse meshes with elements much larger than the sheet thickness itself. The simple BWH expression may therefore be a cost effective and consistent alternative to more complex failure criteria.

Being an instability criterion, the BWH criterion avoids analysis in the post necking zone. This makes the finite element solution less sensitive to the element size, since excessive straining within local necks is avoided. Physically, the use of instability criteria in crashworthiness analysis can be justified by the fact that the remaining energy dissipation within the narrow neck is low compared to the total deformation energy.

Acknowledgments

The EU program: Decision Support System for Ships in Degraded Condition (DSS_DC), is gratefully acknowledged for the economical support of H. S. Alsos. R. Törnqvist expresses his gratitude to Professor Atkins at the University of Reading for the use of the "Giant bulge" in 2001.

References

Arrieux, R., Bedrin, C., Boivin, M., 1982. Determination of an intrinsic forming limit stress diagram for isotropic metal sheets. In: Proceedings of the 12th Biennial Congress IDDRG, pp. 61–71.

Barata da Rocha, A., Barlat, F., Jalinier, J.M., 1985. Prediction of the forming limit diagram of anisotropic sheets in linear and non-linear loading. Materials Science and Engineering 68, 151–164.

Belytschko, T., Lin, J.I., Tsay, C., 1984. Explicit algorithms for the nonlinear dynamics of shells. Computer Methods in Applied Mechanics and Engineering 42, 225–251.

Belytschko, T., Liu, W.K., Moran, B., 2004. Nonlinear Finite Elements for Continua and Structures. John Wiley, LDT.

Bressan, J.D., Williams, J.A., 1983. The use of a shear instability criterion to predict local necking in sheet metal deformation. International Journal of Mechanical Science 25, 155–168.

Brunet, M., Clerc, P., 2007. Two prediction methods for ductile sheet metal failure. In: ESAFORM Conference on Material Forming.

Brunet, M., Morestin, F., 2001. Experimental and analytical necking studies of anisotropic sheet metals. Journal of Materials Processing Technology 112, 214–226.

Cockcroft, M.G., Latham, D.J., 1968. Ductility and the workability of metals. Journal of the Institute of Metals.

Ghosh, A.K., Laukonis, J.V., 1976. The influence of strain path changes on the formability of sheet steel. In: 9th Biennial Congress of the IDDRG, Sheet Metal Forming and Energy Conservation. ASM Publication.

Goodwin, G.M., 1968. Application of strain analysis to sheet metal forming in the press shop. In: SAE paper 680093.

Graf, A.F., Hosford, W.F., 1993. Calculations of forming limit diagrams for changing strain paths. Metal Transactions A 24, 2497–2501.

Graf, A.F., Hosford, W.F., 1994. The influence of strain-path changes on forming limit diagrams of al 6111 t4. International Journal of Mechanical Sciences A36, 897–910.

Gronostajski, J., Dolny, A., Sobis, T., 1982. 12th International Deep Drawing Research Group. In: Congress San Margherita, May 24–28.

Hallquist, J., 2007a. Ls-dyna keyword users manual—ls971. Technical report, Livemore Software.

Hallquist, J., 2007b. Ls-dyna theory manual— ls971. Technical report, Livemore Software.

Hill, R., 1950. The Mathematical Theory of Plasticity. Oxford University Press, London.

Hill, R., 1952. On discontinuous plastic states with special reference to localized necking in thin sheets. Journal of the Mechanics and Physics of Solids 1, 19–30.

Keeler, S.P., Backhofen, W.A., 1964. Plastic instability and fracture in sheet stretched over rigid punches. ASM Transactions Quarterly 56, 25–48.

Marciniak, Z., Kuczynski, K., 1967. Limit strains in processes of stretch forming sheet metal. Journal of Mechanical Sciences 9, 609–620.

Rice, J., Tracey, D., 1969. On the ductile enlargement of voids in triaxial stress fields. Journal of the Mechanics and Physics of Solids 17, 201–217.

Stoughton, T.B., 2000. A general forming limit criterion for sheet metal forming. International Journal of Mechanical Science 42, 1–27.

Stoughton, T.B., 2001. Stress-based forming limits in sheet metal forming. Journal of Engineering Materials and Science 123, 417–422.

Stoughton, T.B., Zhu, X., 2004. Review of theoretical models of the strain-based fld and their relevance to the stress-based fld. International Journal of Plasticity 20, 1463–1486.

Tarrett, Stoughton, T., 2003. Stretch-bend forming limits of 1008 ak steel. In: SAE 2003 World Congress and Exhibition, Detroit, MI, USA.

Törnqvist, R., 2003. Design of crashworthy ship structures. Ph.D. thesis, DTU.

Wu, P.D., Graf, MacEwen, S.R., Lloyd, D.J., Jain, M., Neale, K.W., 2005. On forming limit stress diagram analysis. International Journal of Solids and Structures 42, 2225–2241.